ANALYZING THE SKIMMING PROCESS OF AN ICP-MS USING A MONTE CARLO SIMULATION

by

Adam Payne

A senior thesis submitted to the faculty of

Brigham Young University

in partial fulfillment of the requirements for the degree of

Bachelor of Science

Department of Physics and Astronomy

Brigham Young University

August 2007

BRIGHAM YOUNG UNIVERSITY

DEPARTMENT APPROVAL

of a senior thesis submitted by

Adam Payne

This thesis has been reviewed by the research advisor, research coordinator, and department chair and has been found to be satisfactory.

Date	Ross Spencer, Advisor
Date	Eric Hintz, Research Coordinator
Date	Ross Spencer, Chair

ABSTRACT

ANALYZING THE SKIMMING PROCESS OF AN ICP-MS USING A MONTE CARLO SIMULATION

Adam Payne

Department of Physics and Astronomy

Bachelor of Science

An implementation of the Direct Simulation Monte Carlo Method has been used to model the behavior of the argon background gas in an Inductively Coupled Plasma-mass spectrometer as it expands supersonically from the sampler cone towards the skimmer cone. Of particular interest is the production of a shock wave as the neutral gas flows through the nozzle and expands into the downstream vacuum region. Simulations where the skimmer cone is placed well inside the zone of silence will be presented. The results will show that collisional effects from the skimmer cone can trigger a shock in front of the cone. The results will also show that specularly reflecting (frictionless) cones do not produce a shock structure in front of the nozzle. In each simulation, the overall skimming process will be analyzed. Finally, a simulation using a combination of thermal and specular reflections will be presented in a preliminary attempt to more accurately model gas interaction with the cone surfaces.

ACKNOWLEDGMENTS

There are many people who's help and support made this project possible. I would like to thank my advisor Dr. Ross Spencer for letting me be a part of his research team these past two years. He has spent countless hours helping me understand difficult concepts and eliminating the most invisible 'bugs'.

I would also like to thank my colleagues Jaron Krogel, Jamie Palmer, Andrew Sampson, William Somers and Charlie Woods. Their help and friendship was invaluable.

A special thanks goes to my parents for the love and support they have constantly shown me throughout my many years in college. Last of all, my deepest thanks goes to my wife, whose loving presence I cherish more than anything else.

Contents

Table of Contents **vi**

List of Figures **vii**

1 Introduction **1**
1.1 Historical Context and Perspective 1

2 Computational Setup **5**
2.1 Fluid Dynamics vs DSMC 5
2.2 DSMC 7
2.3 FENIX Geometry 7
2.4 Data Collection 9

3 Results and Conclusion **11**
3.1 Specularly Reflecting Sampler Cone 12
3.2 Thermally Reflecting Sampler Cone 13
3.3 Adding the Skimmer Cone 14
3.4 Specular Reflecting Skimmer Cone 19
3.5 Thermal-Specular Reflecting Skimmer Cone 23
3.6 Conclusion and Future Considerations 29

Bibliography **30**

Index **32**

List of Figures

1.1 Inductively Coupled Plasma Mass Spectrometer 2
1.2 Shock Structure 3

2.1 Mean Free Path and Knudsen Number along the z-axis 6
2.2 FENIX geometry 8
2.3 Comparing the small geometry with the downstream geometry 10

3.1 Shock Structure 11
3.2 Radial Pressure Scans for Specular Reflection 13
3.3 Position of Radial Pressure Scans 13
3.4 Axial Pressure for Specular Reflection 14
3.5 Contour Plot of the Temperature for Specular Reflection 14
3.6 Radial Pressure Scans for Thermal Reflections 15
3.7 Position of Radial Pressure Scans for Thermal Reflections 15
3.8 Axial Pressure for Thermal Reflections 15
3.9 Contour Plot of the Temperature for Thermal Reflections 15
3.10 Comparing the Specular and Thermal Centerline Pressures 16
3.11 Axial Velocity for Thermal Reflection with the Skimmer 17
3.12 Centerline Temperature for Thermal Reflection with the Skimmer . . 17
3.13 Axial Pressure for Thermal Reflection with the Skimmer 18
3.14 Temperature Contours for Thermal Reflection with the Skimmer . . . 18
3.15 Streamline Flow of the Gas Through the Skimmer 19
3.16 Radial Scan of the Density for Thermal Reflection with the Skimmer 19
3.17 Axial Velocity Distribution Upstream from the Thermal Skimmer . . 20
3.18 Axial Velocity Distribution inside the Thermal Skimmer 20
3.19 Axial Velocity Distribution Downstream from the Thermal Skimmer . 20
3.20 Axial Velocity for Specular Reflection 21
3.21 Centerline Temperature for Specular Reflection with the Skimmer . . 21
3.22 Axial Pressure for Specular Reflection with the Skimmer 22
3.23 Temperature Contours for Specular Reflection with the Skimmer . . . 22
3.24 Streamline Flow of the Gas Through the Specular Skimmer 23
3.25 Radial Scan of the Density for Specular Reflection with the Skimmer 23
3.26 Axial Velocity Distribution Upstream from the Specular Skimmer . . 23

3.27 Axial Velocity Distribution inside the Specular Skimmer 24
3.28 Axial Velocity Distribution Downstream from the Specular Skimmer . 24
3.29 Axial Velocity for Thermal/Specular Skimmer 26
3.30 Centerline Temperature for the Thermal/Specular Skimmer 26
3.31 Axial Pressure for Thermal/Specular Skimmer 26
3.32 Temperature Contours for Thermal/Specular Skimmer 26
3.33 Streamline Flow of the Gas Through the Skimmer 27
3.34 Radial Scan of the Density for Thermal/Specular Skimmer 27
3.35 Axial Velocity Distribution Upstream from the Skimmer 27
3.36 Axial Velocity Distribution inside the Skimmer 28
3.37 Axial Velocity Distribution Downstream from the Skimmer 28

Chapter 1

Introduction

1.1 Historical Context and Perspective

The Inductively Coupled Plasma - Mass Spectrometer (ICP-MS, see Fig 1.1) is a machine capable of detecting and measuring trace elements. Applications of the ICP-MS include urine testing and water sampling for metal toxins. These elements may be found in concentrations as low as 1 part in a 100 trillion. A crucial design component in the ICP-MS is the interface between the sampler cone and the skimmer cone, which is designed to deliver a coherent, undisturbed beam of ions toward the mass spectrometer. However, this ideal situation has proven difficult to obtain. In the beginning, sampling cones had diameters of roughly 0.05 mm. This often led to the cone becoming plugged by the analyte solution. Even before the cone became plugged, problems arose with the composition of the plasma beam from its interaction with a relatively cool sampling cone. As the hot gas comes into contact with the cool cone, it produces a boundary layer along the surface of the throat that is rich with chemical reactions. Sampling from this boundary layer, which could have an estimated 10^6 collisions/ms [1], considerably alters the composition of the plasma.

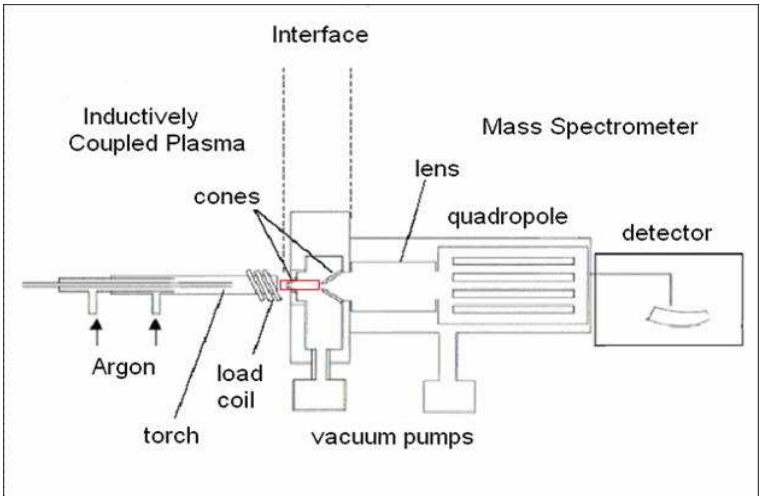

Figure 1.1 Inductively Coupled Plasma Mass Spectrometer.

Work done by Gray and Date [2] show that a larger orifice correctly samples the bulk plasma instead of the boundary layer. Unfortunately, this obvious solution gives birth to new problems. As the plasma expands supersonically through the sampler, a shock structure is formed as the gas plows into the low-pressure background gas. The classic shock structure, including the barrel shock and Mach disc, is shown in Fig 1.2. The barrel shock and the Mach disc (regions of high density) serve to encapsulate a region of undisturbed, low density, supersonic flow. This region is known as the zone of silence and is characterized by M $\gg$ 1, where M = v/c_{sound}, and where v is the speed of the gas, and c_{sound} is the speed of sound. Simple models predict that ideal skimming is achieved when a skimmer cone is placed within this region of undisturbed, supersonic flow.

Much of the theoretical understanding behind the ICP-MS and bulk sampling of plasmas comes from Douglas and French [3] . In their research they cite the relationship:

$$X_m = 0.67 D_0 \sqrt{\frac{P_0}{P_1}} \tag{1.1}$$

where X_m is the distance from the orifice to the Mach disc, D_0 is the orifice diameter,

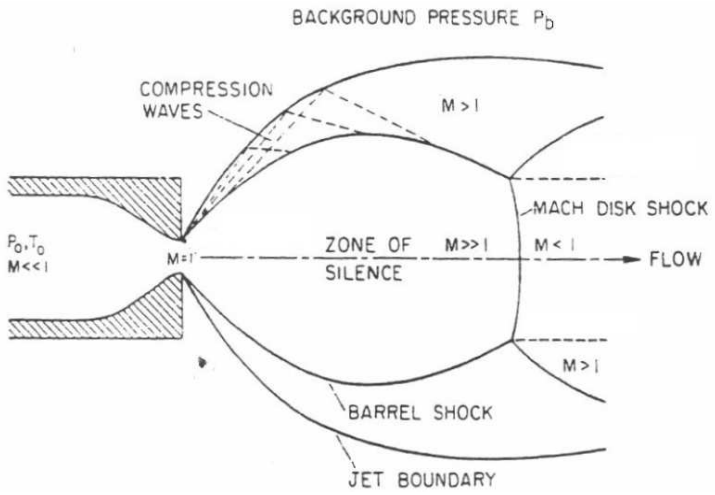

Figure 1.2 Shock Structure

P_0 is the upstream pressure and P_1 is the background pressure in the first expansion region. Equation 1.1 came from experimental work done by Bier and Schmidt. [4] Experiments that support the feasibility of bulk sampling of plasmas were done by Fraser *et al.* [5] However these experiments were performed under very different conditions and measured using techniques that are incompatible with the ICP-MS. For example, the sampler orifice used by Fraser *et al* had a diameter of 44.5 mm which is much larger than the 1 mm diameter holes used in the ICP-MS. In addition, the argon gas expanded into a wind chamber held at 8.380 torr, compared to the 2-3 torr pressure found in the ICP-MS. Thus, another study of the shock structure and the skimming process is needed in order to better understand how the ICP-MS works.

This paper will show the results of a computational simulation (a Direct Simulation Monte Carlo or DSMC program called FENIX [6]) of the shock structure formed downstream from the sampler cone. Specifically, collisional effects on the shock structure and the skimming process from frictionless cones and thermally reflecting cones will be presented. The first two simulations will not have the skimmer cone in place and will serve to locate the zone of silence. Next, simulations of the downstream re-

gion with the skimmer cone well within the zone of silence will be shown. The results will show that a thermally reflecting skimmer cone triggers the formation of a shock structure at the entrance of the skimmer which causes the gas to diverge from the centerline axis. The velocity distribution of the gas at the entrance of the skimmer cone will be compared to experimental results. Simulations will also show that a specularly reflecting or frictionless skimmer cone does not produce a shock structure in front of the skimmer and therefore improves the overall skimming process. Finally, a simulation that combines thermal and specular reflections will be presented. This is a preliminary attempt to more accurately model the gas interaction with the sampler and skimmer cones.

Chapter 2

Computational Setup

2.1 Fluid Dynamics vs DSMC

In building a computational model of the ICP-MS, there are many different approaches. Two popular ones are Fluid Dynamics (solving the Navier-Stokes equations) and Direct Simulation Monte Carlo (uses kinetic theory of gases). In using the Navier-Stokes equations, the fluid is assumed to be continuous. Even though the fluid contains discrete, individual particles that collide with each other and reflect from walls, the fluid is dense enough to have continuous values of temperature, pressure, and density everywhere. DSMC, on the other hand, simulates groups of particles as discrete entities and allows each to move and collide. It then uses statistical sampling to obtain physical quantities. The deciding factor in choosing an approach is the Knudsen number:

$$K_n = \frac{\lambda}{L} = \frac{1}{\sqrt{2} n \sigma L} \tag{2.1}$$

where λ is the local mean free path, n is the local density, σ is the cross-sectional area, and L is the length scale. As shown in Eq. 2.1, the Knudsen number is the ratio between the mean free path of the molecules and the length scale L over which the

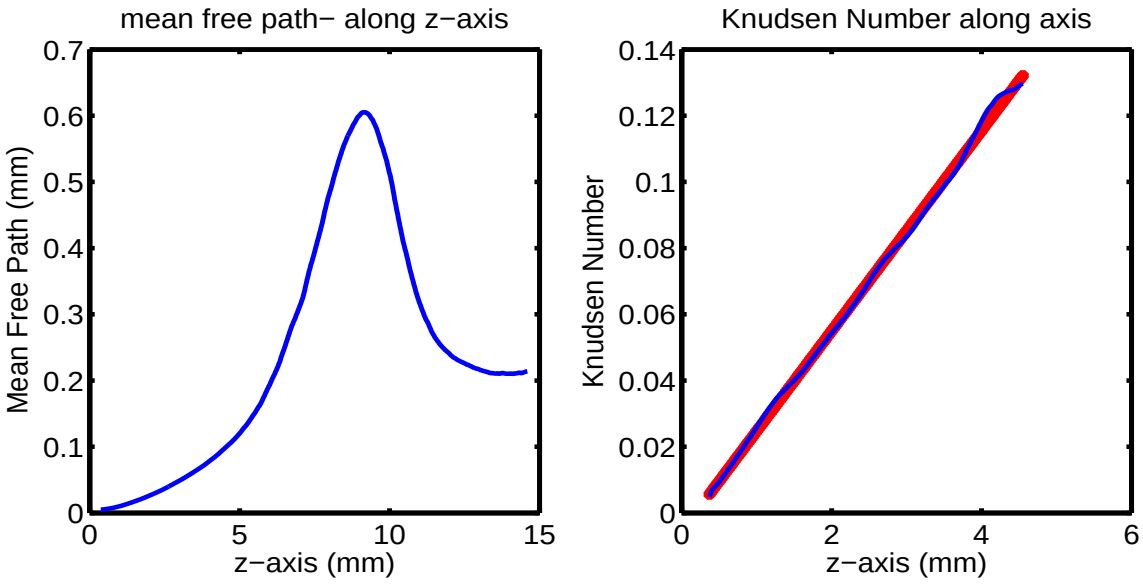

Figure 2.1 Mean Free Path and Knudsen Number along the z-axis

flow changes. The Navier-Stokes equations assume the Knudsen number to be much less than one. As the Knudsen number approaches 0.1 and beyond, the fluid equations break down and kinetic theory must be applied to the problem. To choose between these two approaches then, we must find the Knudsen number in the expansion region. A simple way to do this is to use simulation results. The density was found by averaging over the first five radial cells along the entire z-axis to produce an average axial density. The collision cross section of argon is not constant, but it changes only slightly from its value of 2.66e-19 m^2. Finding the scale length L was slightly more difficult because it is defined as the distance over which the flow changes. L was therefore approximated by finding the ratio between the density and the change in density along the z-axis:

$$L = \frac{n}{\frac{\partial n}{\partial z}} \tag{2.2}$$

In Fig 2.1, the Knudsen number is shown to linearly increase beyond 0.1, the point where fluid theory breaks down. (z=0 is at the end of the throat of the nozzle) For

this reason, DSMC is expected to model the ICP-MS better than the fluid equations.

2.2 DSMC

DSMC is a computational model that comes from kinetic theory and was largely developed by Graham Bird in the 1960's. DSMC is the algorithm used in the FENIX simulation. Each simulation particle represents a large number of real particles. Particles are completely described by their three spatial coordinates and three velocity components. The simulation runs through a series of time steps during which particles move and collide. The basic sequence is

1) move all the particles in the direction of their velocities.

2) sort all the particles into collision cells.

3) randomly choose pairs of particles in each cell to collide based on their relative velocities and the local density.

2.3 FENIX Geometry

Inside FENIX, the basic sequence of DSMC is relatively simple, while the boundary conditions are far more challenging to implement. FENIX uses a cylindrical geometry in two dimensions(axial symmetry). The simulation region with the sampler and boundary conditions are shown in Fig 2.2. For some runs, the sampler cone is kept at a constant temperature of 1500 K and thermally reflects particles that strike it. The particles are re-emitted at a thermal speed calculated using the temperature of the cone and in a random direction evenly distributed over a hemisphere (2π steradians). For other runs, the sampler come specularly reflects the particles that strike it. The particles are re-emitted at the same speed with which they strike the surface and in

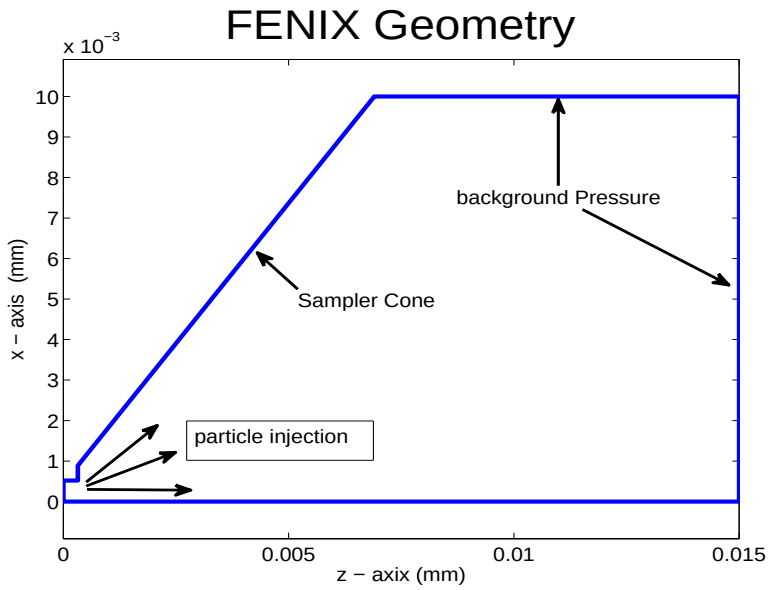

Figure 2.2 This is the FENIX geometry.

a direction found by using specular reflection. The downstream background pressure is produced by specularly reflecting a specified percentage of particles that leave the simulation region downstream. That percentage was calibrated until the desired background pressure was obtained. For each run, radial pressure scans showing the background pressure along all sides of the shock structure will be presented.

Ideally, a model of the ICP-MS would include both the upstream and the downstream regions together. However, this would require a number of collision cells that are computationally unattainable. In order for DSMC to produce accurate statistics, the collision cells must be smaller than the local mean-free-path, and there must be at least 20-25 particles per cell. Our computers do not have the required memory and capabilities necessary to model both the upstream and downstream regions together, because of the numerous collision cells required and the particles needed to fill them. Therefore, the injection of particles into the downstream region came from a separate FENIX simulation of the upstream region. As particles exited the throat

of the sampler in the upstream simulation, their position and velocities were recorded and later used as the injection routine for the downstream region. In order to make sure that the data from the upstream region agreed with the downstream region, a smaller simulation of the area just around the sampler cone was made. The physical quantities from this smaller geometry were then compared with the overlapping area from the downstream simulation.

The results are shown in Fig 2.3. Immediately outside the sampler cone, the physical quantities from the downstream simulation show a discrepancy with the smaller geometry simulation within 0.3 mm of the sampler exit. Beyond 0.3 mm from the sampler exit, the downstream simulation produces the same results as the small geometry. The discrepancy just outside the sampler exit can be attributed to the larger collision cells used in the downstream simulation compared to those in the smaller geometry. With a background pressure of 5 torr, the Mach disc (and other flow properties pertinent to this experiment) would be 8.6 mm from the sampler exit and therefore the difference found in the first 0.3 mm is negligible.

2.4 Data Collection

The final subroutine takes care of gathering all physical quantities. Averages such as $\bar{v_x}$, $\bar{v_y}$, $\bar{v_z}$, $\bar{v^2}$, $\bar{v}^2$, etc, are used in computing the physical quantities of interest: temperature, pressure, density, velocity, etc. FENIX uses a uniform spatial grid that is independent of the collision cells and averages the information over specified blocks of time in order to improve the statistics and provide a steady-state picture.

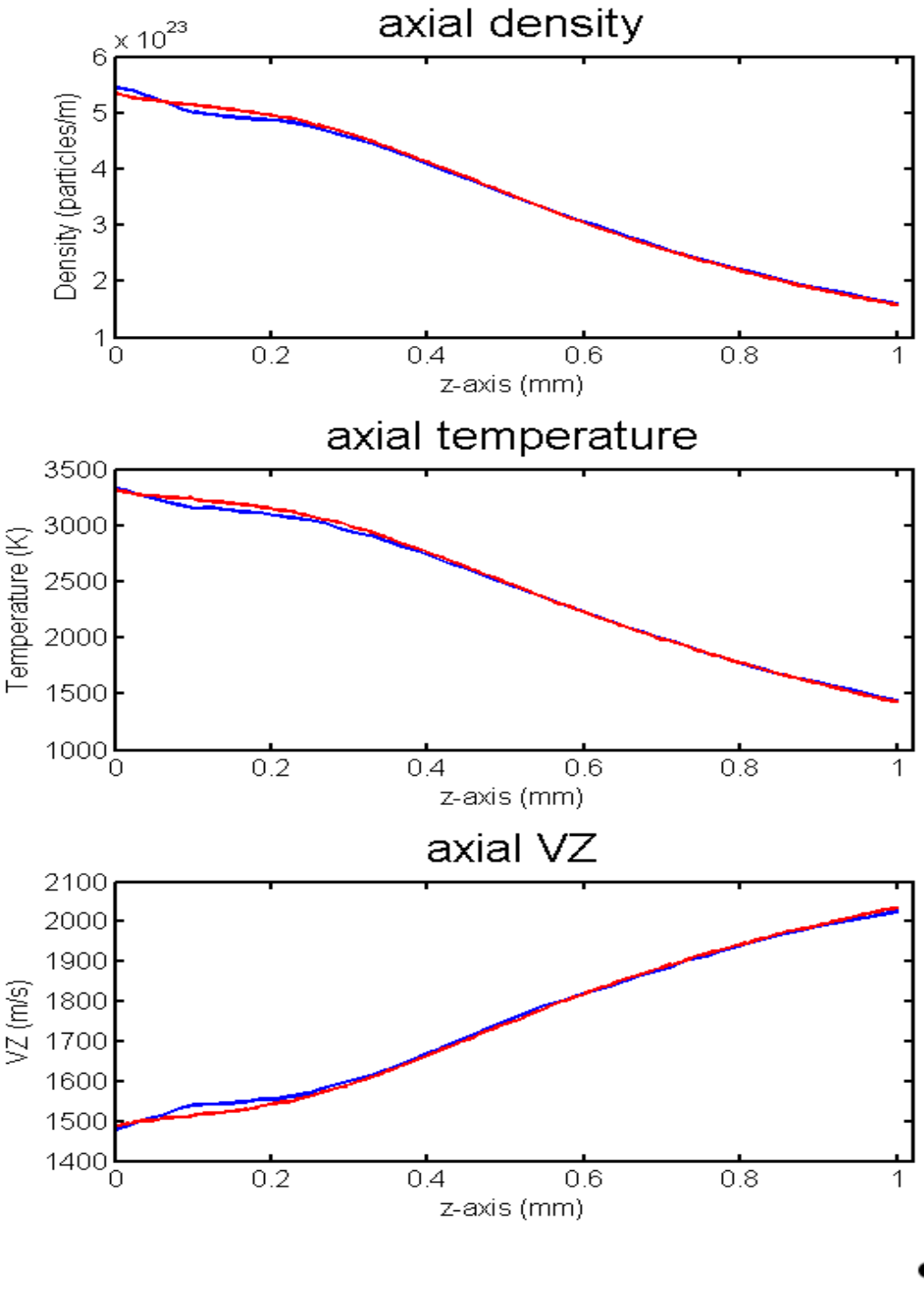

Figure 2.3 Comparison between the small geometry and the downstream geometry. The blue data is the downstream geometry and the red line is the small geometry

Chapter 3

Results and Conclusion

Early work on supersonic expansion was done in giant wind tunnels where gas was directed towards a circular orifice on a vertical plate and allowed to expand into a low pressure chamber. The orifice size was usually around 40 mm and the expansion chamber was held at a pressure of 8 torr. These conditions produce shock structures that have a well defined mach disc, barrel shock, and jet boundary. These structures serve to encapsulate the zone of silence. In the case of the ICP-MS, where the orifice size is 1.04 mm and the downstream pressure is in the mtorr range, we find that the different shock structures are not well defined and cannot be labeled with any accuracy.

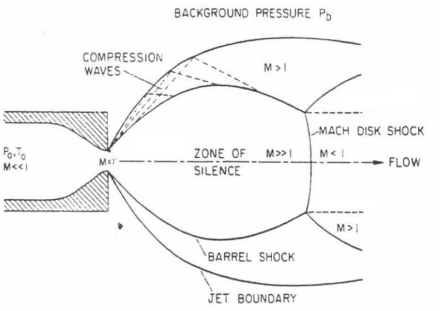

Figure 3.1 Shock Structure

In this chapter, simulations without the skimmer cone will be presented first. These simulations will serve to show the location of the zone of silence which will dictate where the skimmer cone is placed. The next simulations will have the skimmer cone placed well inside the zone of silence. The effects of a thermally reflecting cone versus a specularly reflecting cone will be presented. Specifically, the effects that a cone's temperature has on the shock structure and the ability to achieve ideal skimming will be shown.

3.1 Specularly Reflecting Sampler Cone

This section discusses a simulation whose sampler cone specularly reflects the particles that strike it. This means that particles are re-emitted from the sampler cone at the same velocity at which they strike the surface. Their new trajectories come from a simple reflection calculation. One can tell from Fig. 3.5 that the simulation is indeed using specular reflection since the contour lines approach the sampler at normal angles. This shows that the particles are being reflected at the same temperature at which they strike the cone and hence no thermal boundary layer forms along the edge. The average background pressure above the shock structure can be seen in Fig. 3.2 to be approximately 3.6 torr. Fig. 3.7 shows where each scan in Fig. 3.2 was taken in the geometry. Fig. 3.4 shows the average pressure along the centerline axis and helps to estimate the edge of the zone of silence. The gradual transition from the zone of silence to the background pressure shows that low pressure systems do not produce a definitive mach disc and barrel shock.

Unfortunately, the background pressure is not uniform surrounding the zone of silence and thus Eq. 1.1 becomes difficult to test. The background pressure is higher along axis than it is above the zone of silence. This can be seen indirectly in the

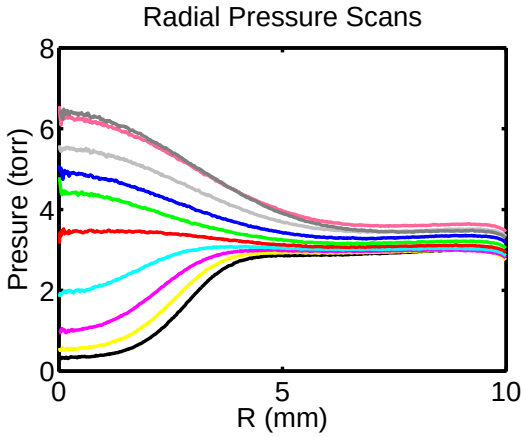

Figure 3.2 Radial Pressure Scans for Specular Reflection

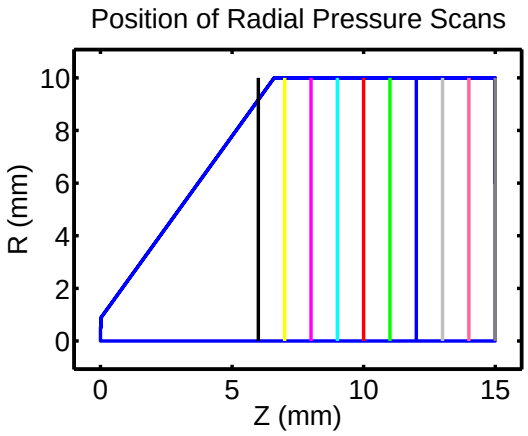

Figure 3.3 Position of Radial Pressure Scans

temperature contour plot where the contour lines near the back of the simulation move closer towards the left as they come down towards the axis. As the temperature increases the background pressure does as well. This is due to how the boundary conditions are being implemented and should someday be remedied so that the background pressure is uniform everywhere along the edge of the zone of silence. This could be done by allowing a smaller percentage of particles to reflect back into the simulation when they are close to the axis than when they are further out. For now, the boundary conditions suffice to produce the background pressure needed for a shock structure.

3.2 Thermally Reflecting Sampler Cone

Here the simulation was run with the cone thermally reflecting the particles that strike it. As particles strike the cone surface, they are re-emitted at a thermal velocity determined by the temperature of the cone. The new direction is randomly chosen over a solid angle between 0 and 2π. The sampler cone is held at a constant temperature

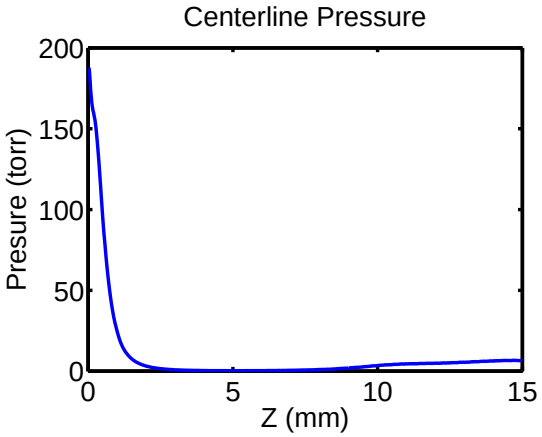

Figure 3.4 Axial Pressure for Specular Reflection

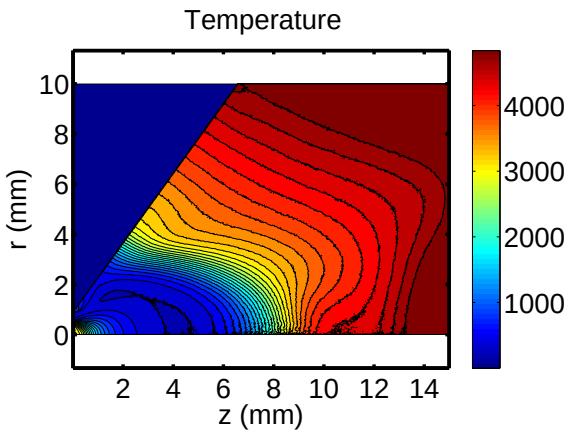

Figure 3.5 Contour Plot of the Temperature for Specular Reflection

of 1500 K and forms a thermal boundary layer along the edge of the sampler cone as seen in Fig. 3.9. The average background pressure above the shock structure can be seen to be approximately 3.3 torr in Fig. 3.6. The centerline pressure again shows a gradual transition from the zone of silence to the background pressure, however this time the transition occurs slightly closer to the sampler than in the specular run.

Fig. 3.10 shows the centerline pressure from both the specular and thermal simulations marked in red and blue lines respectively. (A logarithmic scale was used in order to highlight differences that are hard to see on a linear scale). In the thermal run (blue line), the sampler is cooling the gas in the chamber. As the gas along the axis slightly cools, the pressure also begins to drop and thus extends the length of the zone of silence.

3.3 Adding the Skimmer Cone

The aim of the skimmer cone is to produce a coherent beam of ions that will move towards the mass spectrometer of the ICP-MS. A flow line plot of this 'perfect skim-

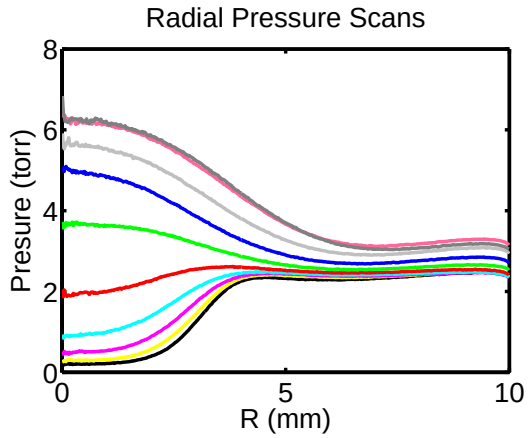

Figure 3.6 Radial Pressure Scans for Thermal Reflections

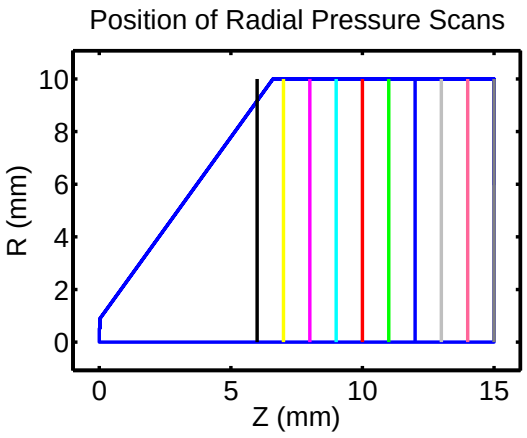

Figure 3.7 Position of Radial Pressure Scans for Thermal Reflections

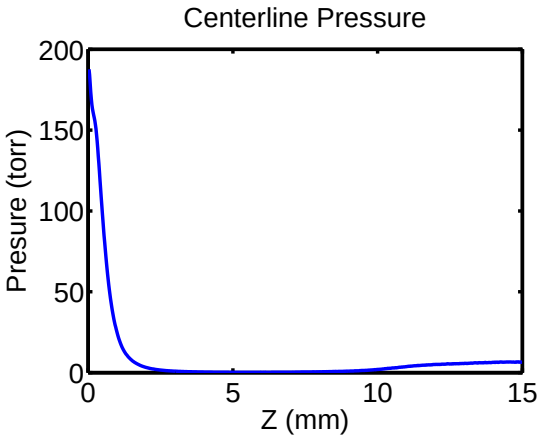

Figure 3.8 Axial Pressure for Thermal Reflections

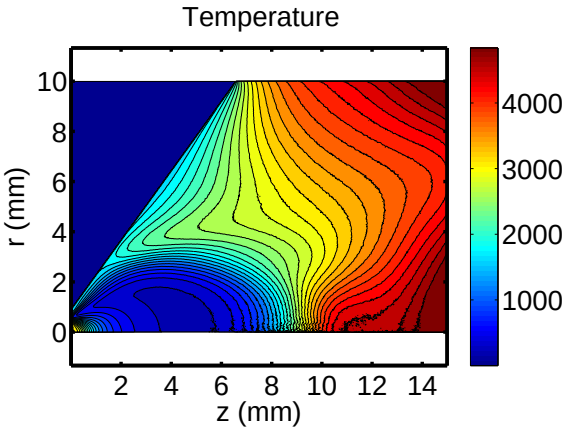

Figure 3.9 Contour Plot of the Temperature for Thermal Reflections

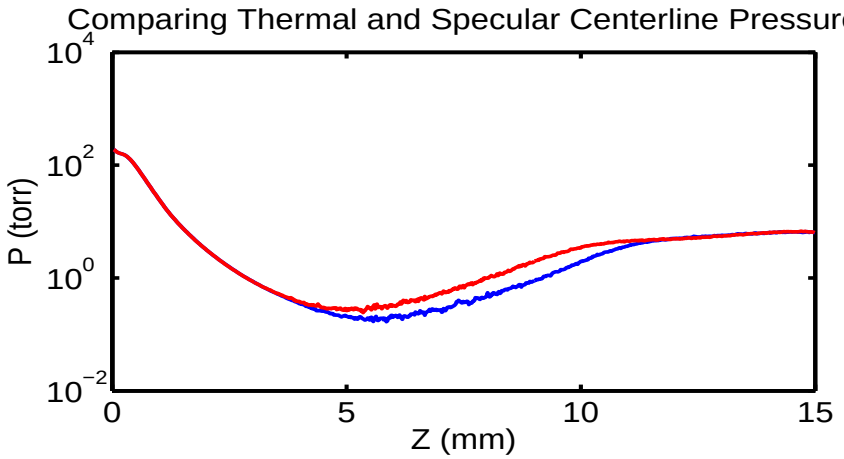

Figure 3.10 Comparing the centerline pressure between the thermal and specular simulations on a log scale. The blue line is the thermal simulation and the red line is the specular simulation.

ming' process would show lines moving past the skimmer without any divergence from the centerline axis. Simple models state that ideal skimming occurs when the skimmer is placed inside the zone of silence so that the edge of the shock structures cannot interfere with the skimming process.

In this simulation, the skimmer cone is placed well within the zone of silence, at a position of 5 mm from the exit of the sampler and with a diameter of 0.68 mm. The skimmer cone is also kept at a constant temperature of 1500 K; as particles strike the cone, they become completely thermalized and are reflected at a randomly scattered solid angle between 0 and 2π steradians. As shown in Fig. 3.11 the gas expands supersonically out of the nozzle. The red bars indicate the entrance and exit of the skimmer throat. The Z velocity peaks inside the zone of silence while the temperature drops to a minimum as all the energy, including any random thermal energy, becomes directed kinetic flow. Through interaction with the skimmer cone, the gas temperature rises (See Fig. 3.12) and its particles are re-emitted with a thermal velocity in a random direction after striking the cone. The heating effect of the skimmer cone causes some of the directed kinetic flow to change back into random

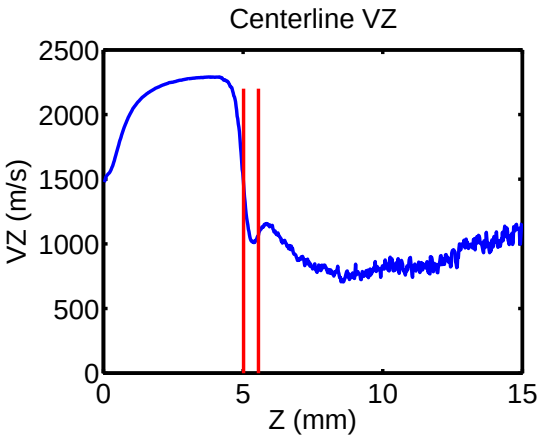

Figure 3.11 Axial Velocity for Thermal Reflection with the Skimmer

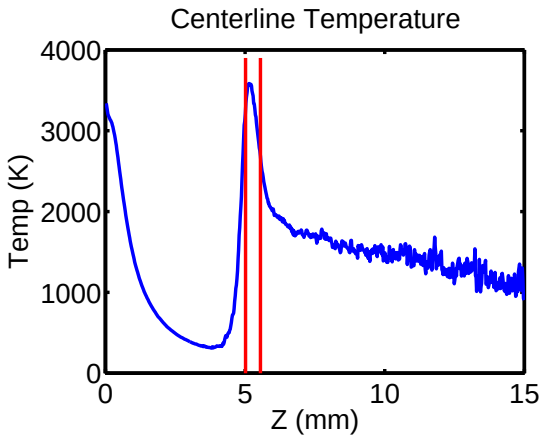

Figure 3.12 Centerline Temperature for Thermal Reflection with the Skimmer

thermal energy which explains the increase in temperature (random thermal energy) and decrease in Z velocity (directed kinetic flow). Fig. 3.11 shows this decrease in VZ as the gas approaches the skimmer tip.

This increase in temperature and the random scattering of particles that strike the cone causes the increase in pressure inside the throat of the skimmer (See Fig. 3.13). This pressure build up exerts a force on the gas that accelerates it through the exit of the nozzle.

The gas moves into another vacuum stage as it exits the skimmer throat. Pressure, density and temperature all steadily drop off while the Z velocity is expected to increase. But for the first few millimeters downstream from the skimmer, the Z velocity actually decreases. This was found by numerical experimentation to be caused by collision effects from the back side of the skimmer. As particles strike the backside of the skimmer, some are reflected towards the axis without further collisions because of their long mean free path.

Instead of producing an axial beam of ions, the gas experiences a secondary ex-

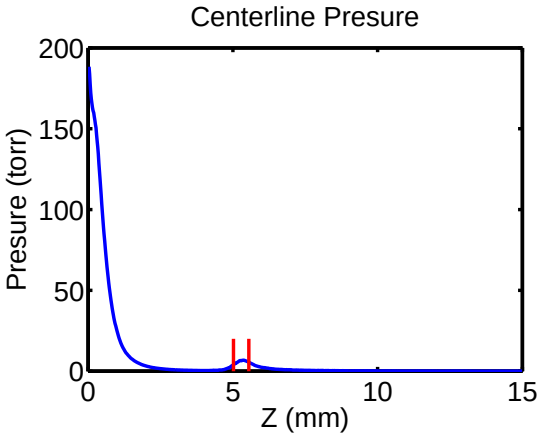

Figure 3.13 Axial Pressure for Thermal Reflection with the Skimmer

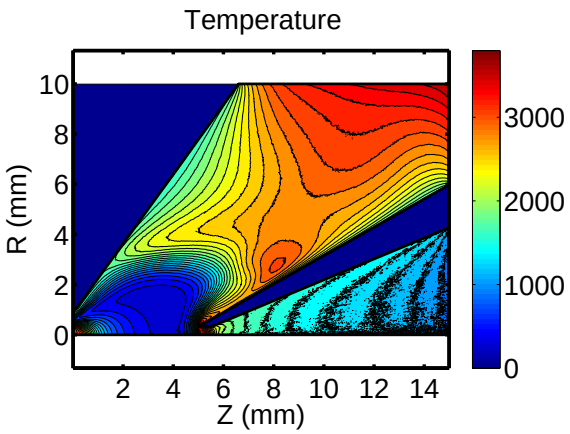

Figure 3.14 Temperature Contours for Thermal Reflection with the Skimmer

pansion as it exits the skimmer throat. This can be seen in Fig. 3.15 as the flow lines spread and diverge away from the axis at all angles instead of all staying horizontal and close to the axis. The red line shows the extent at which ideal skimming would spread from the axis. This secondary expansion is the result of the pressure build up found inside the nozzle. Fig. 3.16 shows a radial scan of the density taken at Z = 12 mm. The density is generally well spread out radially. If ideal skimming took place, the density would drop off considerably in radius. The spreading of the flow lines and the linear radial distribution of density shows that ideal skimming does not take place, even though the skimmer is placed inside the zone of silence.

The shock structure also changes the axial velocity distribution. Figures 3.17 through 3.19 show the axial velocity distribution as the gas moves through the skimmer. The plots on the left show the axial velocity distribution while the plots on the right show the location of the distribution inside the simulation with a red box along the axis. As the gas approaches the skimmer, it is distributed as a single maxwellian with a high flow velocity. As it passes through the shock structure the distribution

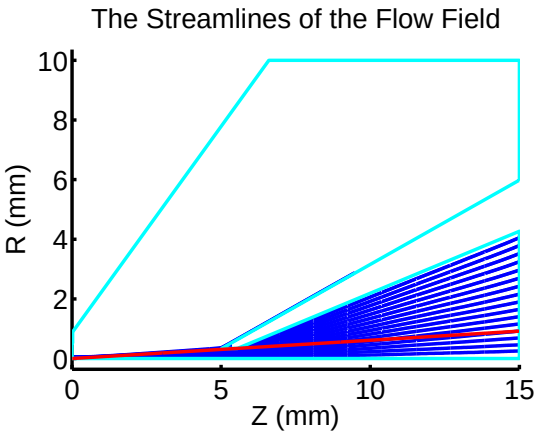

Figure 3.15 Streamline Flow of the Gas Through the Skimmer

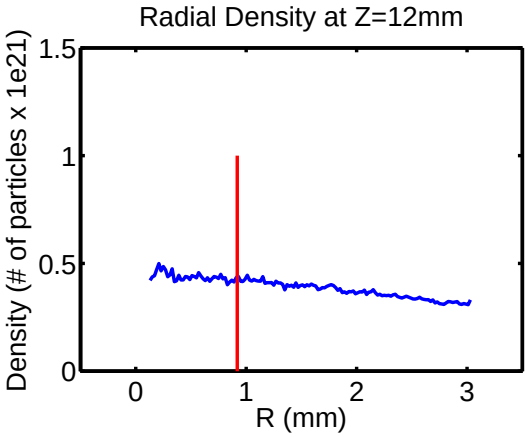

Figure 3.16 Radial Scan of the Density for Thermal Reflection with the Skimmer

splits into a double maxwellian and eventually returns to a single maxwellian further downstream from the skimmer. Mott-Smith showed that this bimodal distribution is a solution of the Boltzmann equation for a shock wave [7]. Experimental work done by Patterson *et al* confirms that a bimodal distribution does in fact form just in front of the skimmer cone. At this time, more specific comparisons cannot be made to the work done by Patterson *et al* [8] because of the different parameters implemented in their experiment versus the parameters made in this simulation (ie. cone temperature, background pressure, sampler-skimmer separation).

3.4 Specular Reflecting Skimmer Cone

While the story of the specular simulation begins much like the thermal simulation, it turns out to have quite a different ending. The gas begins by expanding supersonically into the zone of silence where all of its energy is directed kinetic energy as shown by the high Z velocity in Fig. 3.20. It follows that the temperature drops due to the lack of random thermal energy(See Fig. 3.21). As the gas interacts with the

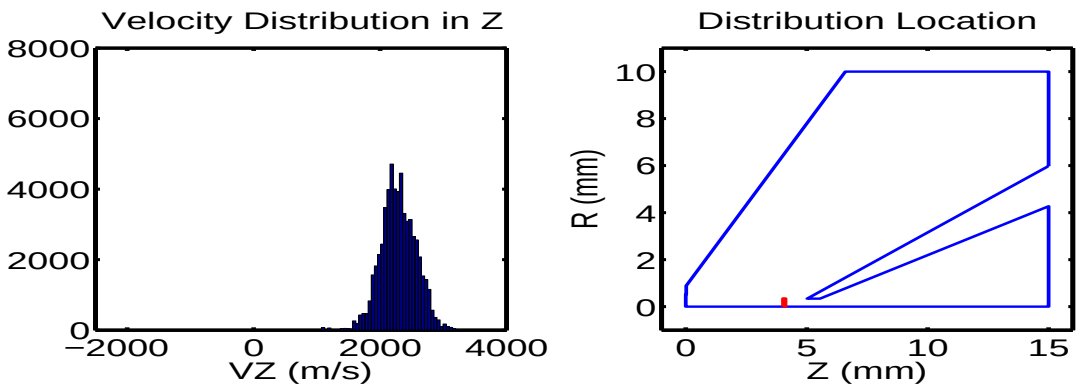

Figure 3.17 Upstream from the Skimmer

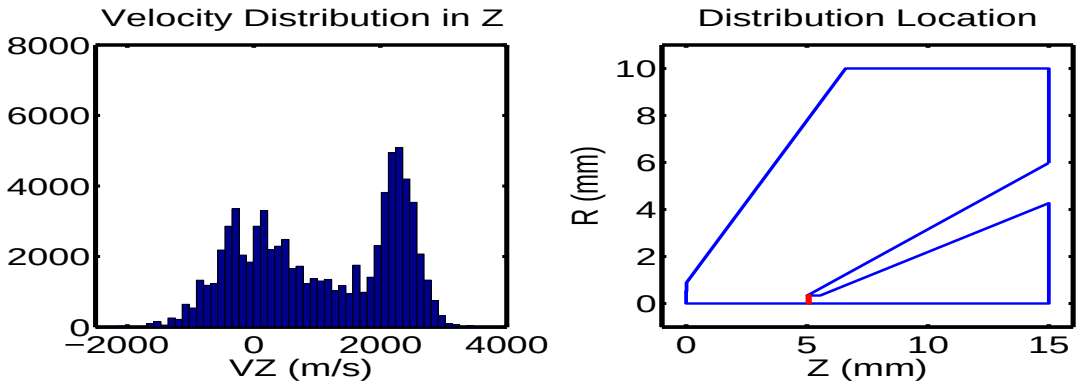

Figure 3.18 Inside the Skimmer

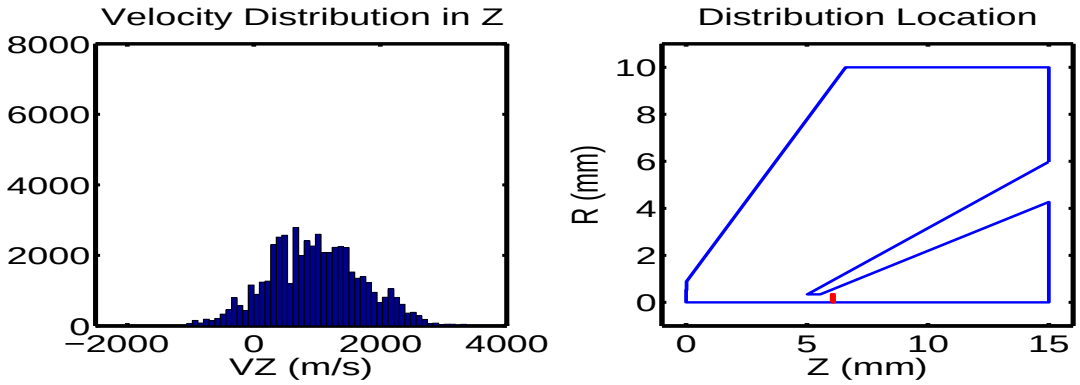

Figure 3.19 Downstream from the Skimmer

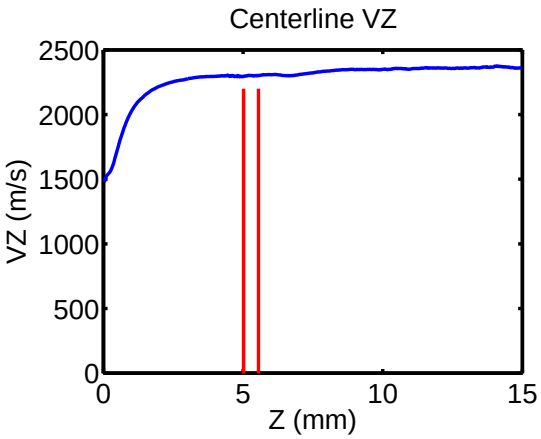

Figure 3.20 Axial Velocity for Specular Reflection

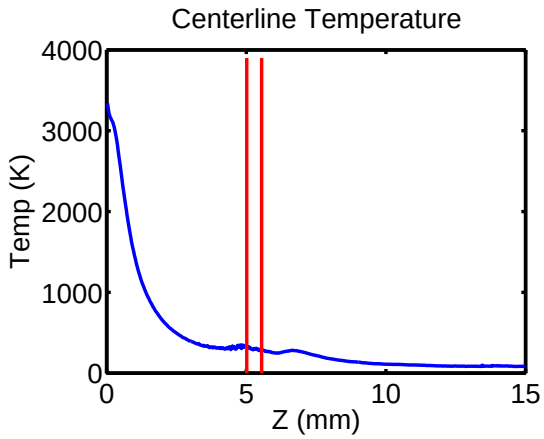

Figure 3.21 Centerline Temperature for Specular Reflection with the Skimmer

skimmer, particles reflect with the same speed that they strike the surface. There are no collision effects from the skimmer to randomize the directed kinetic energy into random thermal energy. Without any new thermalized velocities and random scattering, there is no pressure increase inside the throat of the nozzle (See Fig. 3.22. The centerline temperature does show a slight increase in temperature very close to the entrance of the skimmer and another increase 1.5 mm downstream from the exit. Both come from specular reflections off the cone. The first one comes from reflections near the tip of the sampler where the mean free path of the particles are still small. The second increase comes from specular reflections inside the nozzle near the exit, where particles have a longer mean free path and are being redirected toward the axis.

The temperature increase downstream from the skimmer is actually large enough to have created a slight pressure bulge in the same location. The small pressure bulge(that is too small to see in Fig. 3.22) exerts a small force on the gas that explains the small increase in the Z velocity at Z = 7 mm.

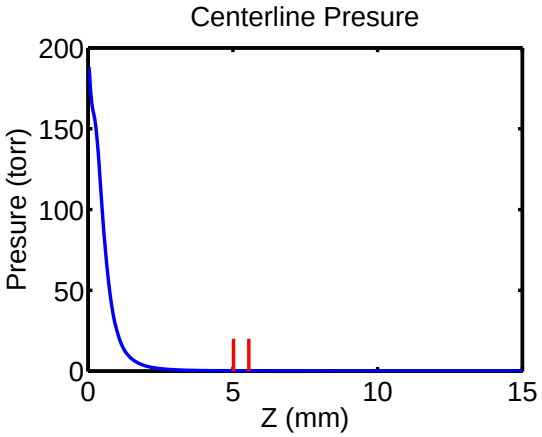

Figure 3.22 Axial Pressure for Specular Reflection with the Skimmer

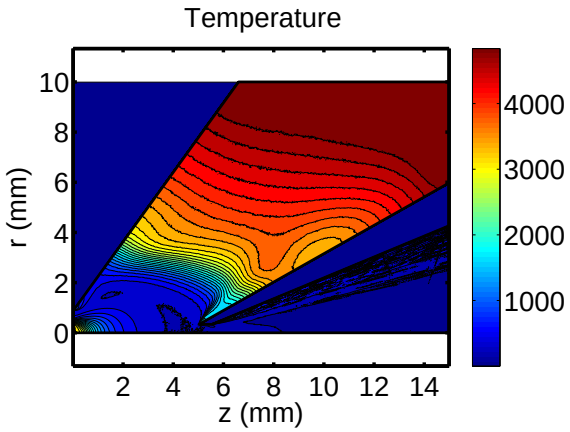

Figure 3.23 Temperature Contours for Specular Reflection with the Skimmer

This time the streamlines stay closer to the axis as a result of the absence of a pressure bulge in the throat of the skimmer. Again the red lines show the extent in which streamlines would spread in the case of ideal skimming. Fig. 3.25 shows that most of the particles remain within the region of ideal skimming. While these graphs show a more focused beam along the axis than the ones produced (or not produced) by the thermal simulation, they do not fully simulate ideal skimming. Fig. 3.25 shows that the density does not come to zero until after the red vertical line which means that ideal skimming is not completely taking place.

Without any major pressure bulge inside the skimmer throat, it is expected that the velocity distribution would not become bimodal. Fig. 3.26 through Fig. 3.28 shows the Z velocity distribution, taken in the same positions as shown in the thermal simulation. Inside the zone of silence, the distribution is centered around a high velocity because all its energy is directed kinetic flow. Inside the skimmer throat, the gas continues to be directed kinetic flow. Because the flow does not change into random thermal energy, the distribution never forms a second maxwellian centered

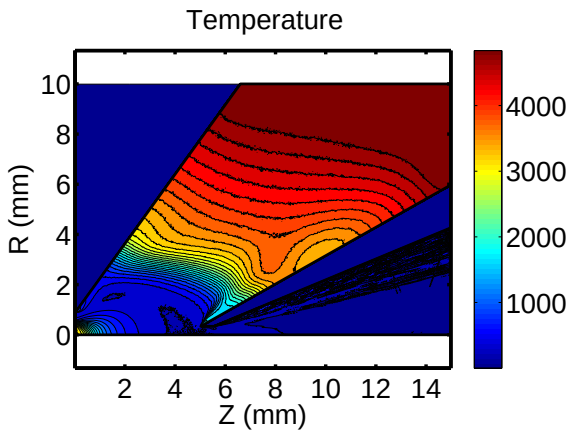

Figure 3.24 Streamline Flow of the Gas Through the Specular Skimmer

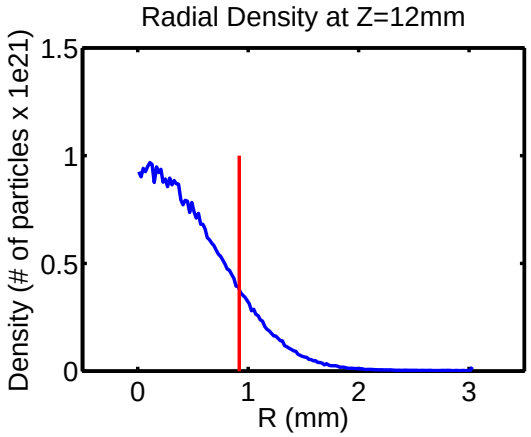

Figure 3.25 Radial Scan of the Density for Specular Reflection with the Skimmer

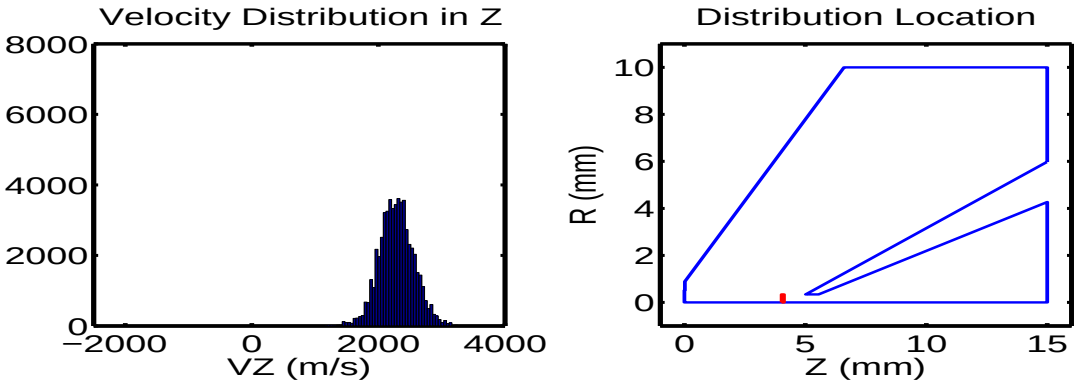

Figure 3.26 Upstream from the Skimmer

around Z velocity of zero.

3.5 Thermal-Specular Reflecting Skimmer Cone

Up to this point, simulations have run with either purely thermal reflections or purely specular reflections. The thermal routine instantly thermalizes a particle after a single strike. Real atoms would normally need a few collisions (at least more than one) with the surface and other particles before they become thermalized. The specular routine

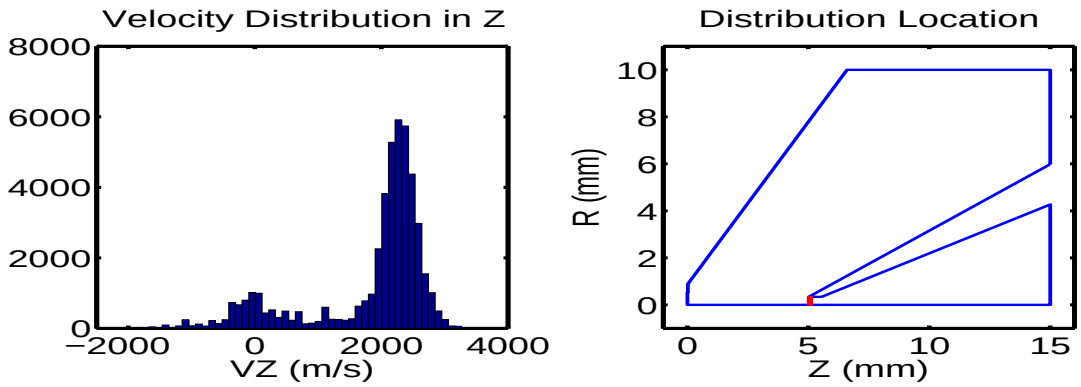

Figure 3.27 Inside the Skimmer

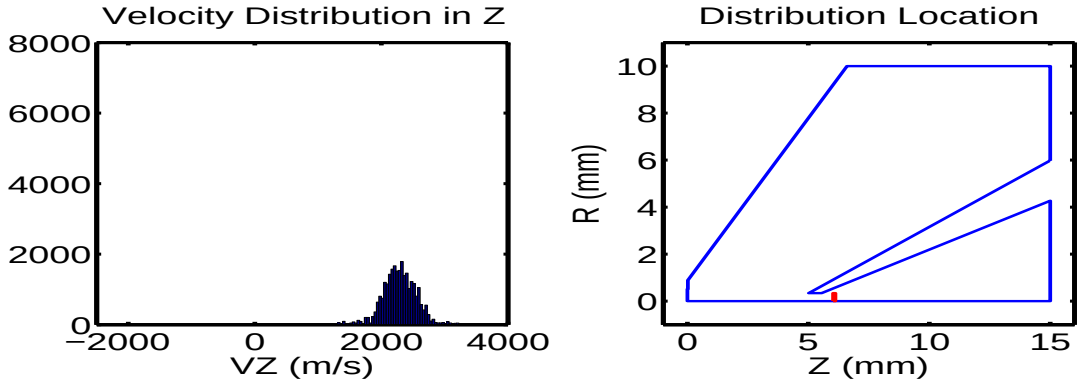

Figure 3.28 Downstream from the Skimmer

assumes the metal surface is perfectly smooth and that the collisions are perfectly elastic. The roughness of the metal surface is many orders of magnitude bigger than argon atoms and therefore the redirected trajectories are not simple reflections. Hence, neither routine accurately describes how gas particles interact with the metal surface. The truth lies, perhaps, somewhere in the middle. A better model would use both thermal and specular reflections.

A simulation was made that utilized both reflection routines on an equal basis. Every time a particle strikes the sampler or the skimmer cone a random number between 0 and 1 decides whether to use thermal reflection or specular reflection. The ratio was set so that half the time thermal reflections would take place and during the other half specular reflections would take place, chosen at random. The 50/50 ratio was arbitrarily selected, and should be compared to experimental results in order to select a more accurate ratio in the future.

Fig. 3.29 shows the gas accelerating into the zone of silence. The Z velocity eventually drops because of collisional interactions with the cone, while the temperature rises (see Fig. 3.30) and produces a pressure bulge inside the throat of the nozzle as shown in Fig. 3.31. Again, the interaction with the skimmer cone shows directed flow energy being converted into random thermal energy. Notice that the pressure bulge reaches a much lower maximum compared to the pressure bulge found in the thermal simulation.

The pressure bulge inside the skimmer throat exerts a force that accelerates the particles past the exit of the skimmer. Fig. 3.29 shows that acceleration. In the thermal simulation, the Z velocity decreased due to thermal reflections just outside the throat of the skimmer. This time the collisional effects from the backside of the skimmer are not strong enough to slow down the flow velocity. Inside the vacuum stage, the Z flow velocity increases, and the temperature and pressure drop steadily.

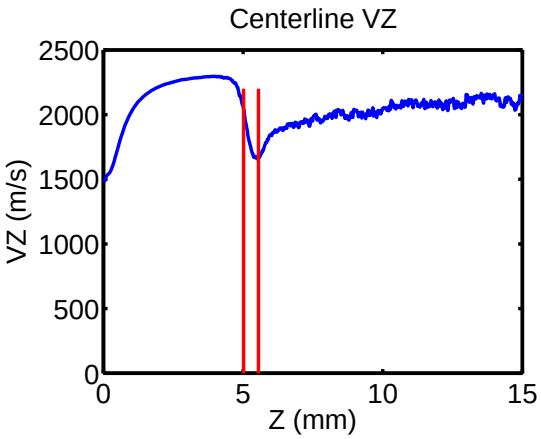

Figure 3.29 Axial Velocity for Thermal/Specular Skimmer

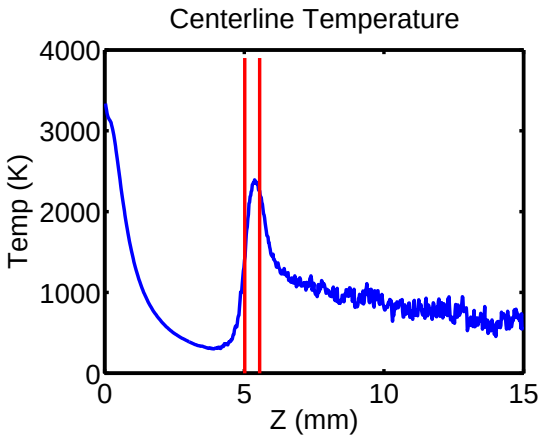

Figure 3.30 Centerline Temperature for the Thermal/Specular Skimmer

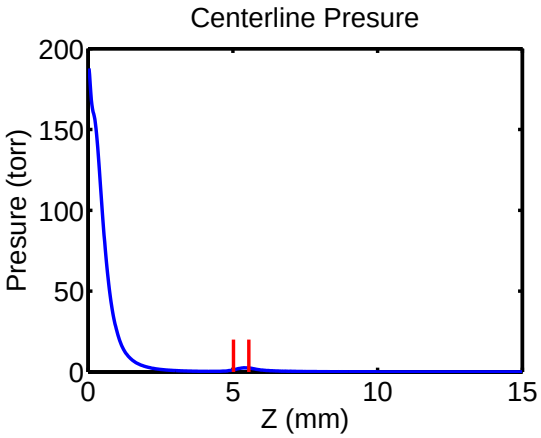

Figure 3.31 Axial Pressure for Thermal/Specular Skimmer

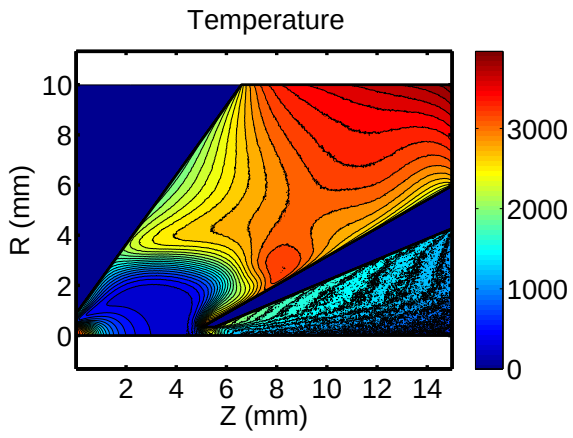

Figure 3.32 Temperature Contours for Thermal/Specular Skimmer

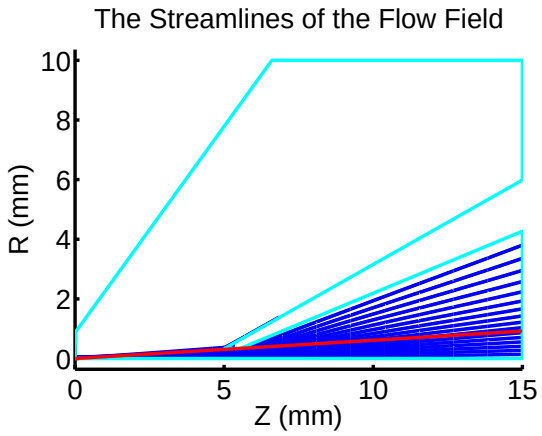

Figure 3.33 Streamline Flow of the Gas Through the Skimmer

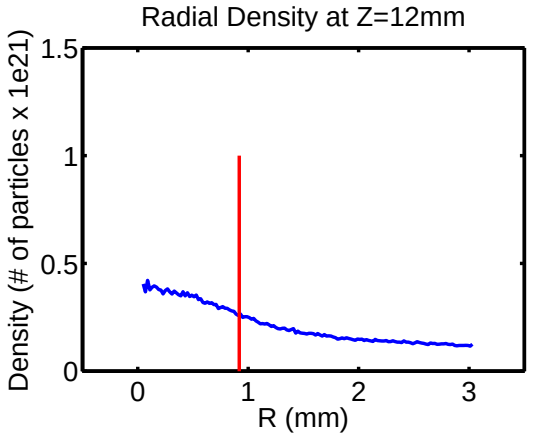

Figure 3.34 Radial Scan of the Density for Thermal/Specular Skimmer

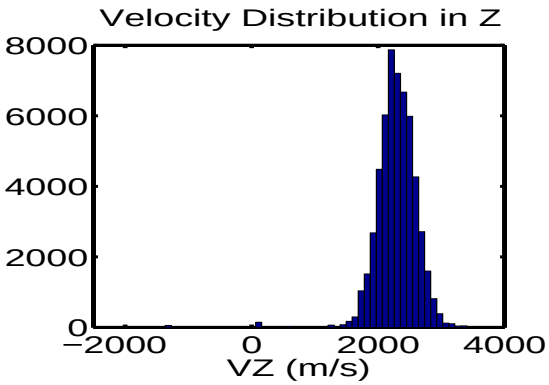

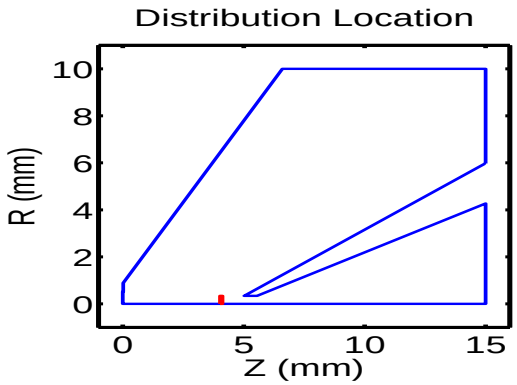

Figure 3.35 Upstream from the Skimmer

The streamlines of the flow field show that particles are being spread throughout the entire downstream region. A more quantitative analysis is shown in Fig. 3.34. It shows that the density drops off more rapidly than was found in the thermal simulation. But unlike the specular simulation, the density is still being spread out at all radii downstream from the skimmer.

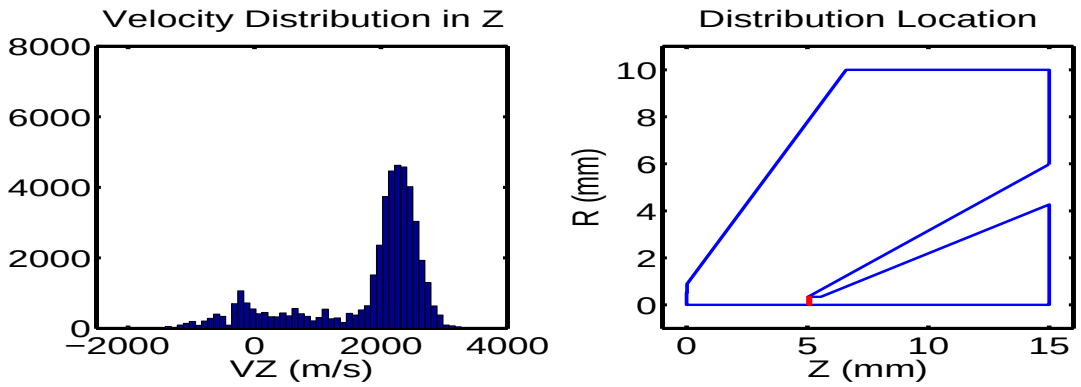

Figure 3.36 Inside the Skimmer

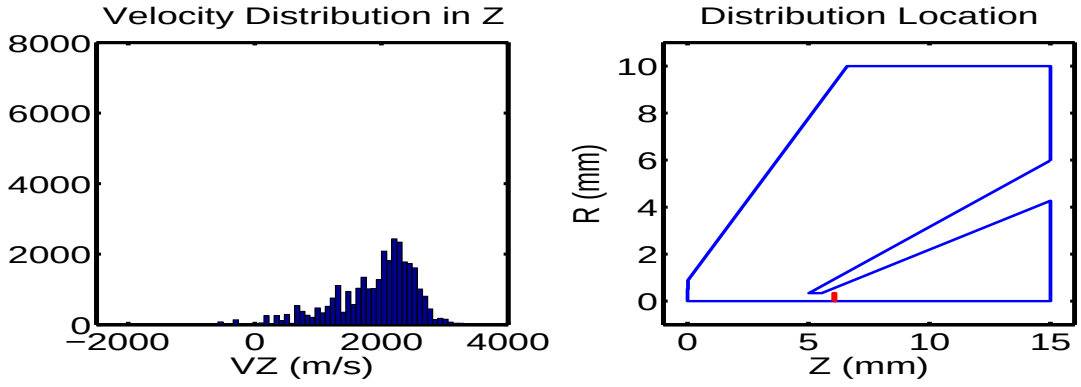

Figure 3.37 Downstream from the Skimmer

3.6 Conclusion and Future Considerations

Simulations of the gas expanding from the exit of the sampler show that there is a zone of silence, but that there is no well defined mach disc or barrel shock. The first simulation without the skimmer had the sampler cone specularly reflecting the particles that strike it while the other simulation had the sampler cone held at a constant temperature of 1500 K and thermally reflecting the particles. The outer edge of the shock structure along the axis begins to form earlier in the specular simulation than in the thermal simulation. This is due to collisional effects from the 'warm' sampler.

The thermal simulation shows that collisional effects from the cone produce a shock structure inside the skimmer throat. This shock structure forms even though the skimmer is placed well within the zone of silence. The pressure bulge inside the throat of the nozzle causes a secondary expansion into the vacuum region. The thermal simulation also shows that a bimodal velocity distribution appears just inside the skimmer throat. Experimental results confirm that a bimodal velocity distribution does exist at the entrance of the skimmer [8].

The specular simulation gives more hopeful results of achieving ideal skimming. Without the collisional effects, a shock structure never forms inside the throat. The flow velocity is able to stay constant throughout the zone of silence and on through the downstream region past the skimmer. Without the shock structure, the skimmer is able to sample the zone of silence more accurately so that the mean free path of the particles is long and particle interaction with each other are minimal. With minimal interactions, the particles continue to move parallel to the axis (instead of diverging away from the axis) and produce a better axial beam. The velocity distribution shows little random thermal energy in the Z velocity.

Finally, the last simulation was a combination of the thermal and specular reflection routines. The ratio between how many specular reflections and thermal reflections take place becomes a parameter that might produce a better model for how gas particles interact with metal surfaces. While the collisional effects were slightly mitigated, they were still the reason for the formation of a smaller shock structure. The velocity distribution still became bimodal and hence a coherent axial beam was not produced.

A lot of future work must still be devoted to this project. The project is currently working closely with experimentalists in the BYU Chemistry Department. Many parameters need to be changed in this simulation in order to compare results with those from the experiments. For instance, this simulation had a sampler-skimmer separation of 5 mm while the experiment has a separation of 10 mm. In the experiment, the system is pumped down to 1 torr. In order to get a 1 torr background pressure that matches the experiment, the simulation region would have to be extended and thus demand much more computational memory. In this simulation, the background pressure is approximately 3.5 torr so that a shock structure will appear in a shorter distance and therefore require less memory. Also, the simulation holds both cones at a constant temperature of 1500 K. The real temperature of the skimmer cone is probably closer to 500 K. While changing the temperature of the cones is a relatively easy change, lowering the background pressure will require a different geometry, and more computing power and memory. The simulation region should also be extended in order to produce a uniform background pressure everywhere along the zone of silence. Finally, many different simulations should be run while changing the thermal/specular parameters. These results should be compared with experimental results in order to obtain a more correct model for how gas particles interact with the cone surfaces.

Bibliography

[1] R. Houk, V. Fassel, G. Flesch, and H. Svec, "Inductively Coupled Argon Plasma as an Ion Source for Mass Spectrometric Determination of Trace Elements," Anal. Chem. 52 (1980).

[2] A. L. Gray and A. R. Date, "Inductively Coupled Plasma Source Mass Spectrometry Using Continuum Flow Ion Extraction," The Analyst 108 (1983).

[3] D. J. Douglas and J. B. French, "Gas Dynamics of the Inductively Coupled Plasma Mass Spectrometry Interface," J. Analytical Atomic Spectromety 3 (1988).

[4] K. Bier and B. Schmidt, Z. angew. Chem. 13 (1961).

[5] R. Fraser, F. Robben, and L. Talbot, "Flow Properties of a Partially Ionized Free Jet Expansion," The Physics of Fluids 14 (1971).

[6] J. T. Krogel, "Simulating the Inductively-Coupled Plasma Mass Spectrometer Using the Direct Simulation Monte Carlo Method," (2006).

[7] H. Mott-Smith, "The Solution of the Poltzmann Equation for a Shock Wave," Phys. Rev. **82,** 885 (1951).

[8] J. Patterson, B. S. Duersch, and P. Farnsworth, Spectrochemica Acta. Part B 54 (1999).

Index

analyte, 1

background pressure, 8, 12, 14, 30
bimodal, 19, 22
boundary conditions, 2, 7
boundary layer, 1, 12, 14

collision cells, 7–9
collisional effects, iv, 29

downstream, iv, 3, 8, 9, 21
DSMC, iv, 3, 5, 7, 8

elastic, 25

FENIX, 7, 8
flow lines, 18
flow velocity, 29

ICP-MS, iv, 1, 8, 14
ideal skimming, 16
ions, 1

Knudsen number, 5

mach disc, 2, 29
maxwellian, 18, 22
memory, 30

Navier-Stokes equations, 5

parameters, 30
plasma, 1
pressure, 21, 25

sampler cone, 7, 9, 12, 13
shock structure, iv, 2, 3, 16, 29
skimmer, 12, 14, 17, 25
specular reflection, 12
specular reflections, 7, 21, 25
statistical mechanics, 5

temperature, 21, 25
thermal reflections, 7, 13, 16, 23, 25

upstream, 8
urine, 1

velocity distribution, 4, 18, 19, 23, 27

wind tunnels, 11

zone of silence, iv, 2, 11, 12, 16, 19, 25, 29